J Solid State Electrochem (1999) 3: 264–276

ORIGINAL PAPER

N.F. Zakharchuk · N. Naumov · R. Stösser
U. Schröder · F. Scholz · H. Mehner

Solid state electrochemistry, X-ray powder diffraction, magnetic susceptibility, electron spin resonance, Mössbauer and diffuse reflectance spectroscopy of mixed iron(III)-cadmium(II) hexacyanoferrates

Received: 12 November 1997 / Accepted: 5 October 1998

Abstract Coprecipitates of Cd^{II}, K^{I} and Fe^{III} with hexacyanoferrate ions $[Fe(CN)_6]^{4-}$ have been studied by solid-state electrochemistry (voltammetry of immobilized microparticles), magnetic susceptibility measurements, X-ray powder diffraction, electron spin resonance, Mössbauer and diffuse reflectance spectroscopy. Most suprisingly, all experimental results point to the formation of a continuous series of complex mixed phases without the formation of phase mixtures. Although Cd^{II} and Fe^{III} ions differ too much in their ionic radii to allow the formation of simple substitution mixed hexacyanoferrates, they are capable of forming different kinds of complex insertion and substitution mixed crystals because of the zeolitic structure of both the iron and the cadmium hexacyanoferrate. Low cadmium concentrations can be found in the zeolitic cavities of iron hexacyanoferrate (Prussian blue), and they start to widen the lattice and facilitate, at higher concentrations, the direct substitution of high-spin iron(III) ions by cadmium ions. In cases of an excess of cadmium, the formation of cadmium hexacyanoferrate with iron(III) ions in the interstitials of the zeolitic structure is observed. These mixed phases show strong charge transfer bands in the visible range and have the appearance of "diluted" Prussian blue. For the first time, this indicates that the charge transfer between the carbon-coordinated low-spin iron(II) ions and the high-spin iron(III) ions can also occur when the latter are situated in the cavities of a host hexacyanoferrate. In Prussian blue the interstitial iron(III) ions are responsible for a very strong charge transfer interaction between the low-spin iron(II) ions and the nitrogen-coordinated high-spin iron(III) ions. Upon substitution of the very small amount of interstitial iron(III) ions in Prussian blue by potassium and cadmium ions the Kubelka-Munk function diminishes by more than 30%, indicating a tremendous decrease in iron(III)-iron(II) interaction.

Key words Solid state electrochemistry · Mössbauer · Magnetic susceptibility · X-ray powder diffraction · Iron(III)-cadmium(II) hexacyanoferrates

N.F. Zakharchuk (✉) · N. Naumov
Institute of Inorganic Chemistry,
Siberian Branch of Russian Academy of Sciences,
Acad. Lavrentyev pr. 3, 630090 Novosibirsk, Russia

R. Stösser · U. Schröder[1] · F. Scholz[1] (✉)
Institut für Chemie, Humboldt-Universität,
Hessische Strasse 1-2, D-10115 Berlin, Germany

H. Mehner
Bundesanstalt für Materialforschung und -prüfung (BAM),
Rudower Chaussee 5, D-12489 Berlin, Germany

Present address:
[1] Institut für Physikalische Chemie,
Ernst-Moritz-Arndt-Universität,
Soldtmannstrasse 23, D-17489 Greifswald, Germany
e-mail: fscholz@rz.uni-greifswald.de,
Tel.: +49-3834-864450, Fax: +49-3834-864451

Introduction

The properties of mixed crystal phases are of great importance in chemistry and physics since situations of wanted or unwanted impurity may lead to their formation. The properties of mixed phases usually deviate from those of the border compounds quite remarkably.

Prussian blue and similar compounds are very well suited for the study of the electrochemical properties of mixed compounds as they exhibit a stable and reversible solid-state electrochemical response. The electrochemistry of electrodes which have been modified by films of Prussian blue or its analogues has been extensively studied, since they are of high interest with respect to electrocatalysis [1], the preparation of ion selective electrodes [2], electrochromism [3–6] and photoelectrochemistry [7]. Additionally, the study of the electrochemistry of solid hexacyanometalates is very important to gain access to the fundamentals of solid-state electrochemistry. The electrochemistry of simple hexacyanoferrates has been studied in particular [8–12]. The

electrochemistry of mixed metal(1)/metal(2) hexacyanoferrates is more complex. However, there are a number of publications dealing with such systems. Mixed hexacyanoferrates also deserve interest, as a tuning of their properties via mixed phase formation is attractive. Siperko and Kuwana [13] studied the electrochemistry and spectroscopy of sandwich layers of Prussian blue on copper hexacyanoferrate. They have reported two different signals of Prussian blue, i.e. the signal of the high-spin iron at 0.2 V and of the $[Fe(CN)_6]^{4-/3-}$ pair at 0.88–0.85 V. The signal of $Cu^{II/I}$ occurs at 0.10–0.12 V and the signal of $[Fe(CN)_6]^{4-/3-}$ of the copper hexacyanoferrate at 0.76–0.72 V. The cathodic peak of the latter system is absent when copper hexacyanoferrate is formed on top of Prussian blue. Bharathi et al. [14] studied the behaviour of mixed iron-nickel and iron-manganese hexacyanoferrate films on glassy carbon. In the case of the iron-nickel system, they have observed four redox processes at −0.10, 0.19, 0.58 and 0.85 V. With increasing nickel concentrations in the film, they have seen shoulders on both sides of the peak at 0.58 V. In the case of iron-manganese hexacyanoferrate films, they have observed three distinct reversible redox systems at 0.19, 0.65 and 0.85 V. As in the case of the iron-nickel system, the peaks at 0.19 V and 0.85 V were assigned to the redox couples of Prussian blue. The peak at 0.65 V was considered to be caused by the $[Fe(CN)_6]^{4-/3-}$ units of Ni hcf (hereinafter "hcf" denotes "hexacyanoferrrate"). From the results obtained, the authors concluded that the films behave as coprecipitations of the two hcfs, with some of the nitrogen-coordinated high-spin iron(III) ions substituted by nickel or manganese ions. Kulesza and co-workers [15] have obtained films of silver(I)-nickel(II) hcfs by cyclic polarisation of a glassy carbon electrode in colloidal solutions of the appropriate compounds. The authors believe the films to have a cross-linked microstructure. They noticed that they are less permeable than a similar film of Prussian blue. An interesting point is that the differences in the radii of both metal ions ($r_{Ag(I)}$ = 129 pm and $r_{Ni(II)}$ = 83 pm [16]) are much too large to allow the formation of substitution mixed crystals. Unfortunately, they are difficult to obtain on the surface of electrode films with a certain composition and, therefore, it is not easy to relate their electrochemical properties to the composition and structure of the film. The voltammetry of microparticles, which has been introduced by Scholz and co-workers [17, 18], made possible a number of electrochemical studies on well-characterised, chemically synthesised hexacyanometalate samples [19–23]. When increasing the x value in the formula $(Fe_{1-x}M_x)[Fe(CN)_6]$, the formal potential of the hcf system almost linearly shifts from the value of Prussian blue to that of nickel hcf [21]. For pure mixed phase compositions, one observes only one voltammetric system instead of the two systems which can be observed only when both hcfs are present in their pure form. From the thermodynamically controlled behaviour of the mixed systems, the authors have drawn the conclusion that mixed phases have been formed instead of a phase mixture. With respect to the nickel iron system, it is important to note that the difference of the radii is less than 6% [16]. Very recently, the same authors achieved the formation of truly bilayered systems of two metal hcfs by an electrochemically driven substitution mechanism and proved it [22]. Thus, the formation of cadmium hcf on top of Prussian blue and on top of silver hcf has been reported to occur along with the formation of nickel hcf on top of Prussian blue.

In the present paper, the results obtained in a systematic study of the cadmium-iron hcf system, i.e. $(Fe_{1-x}Cd_x)[Fe(CN)_6]$, are reported. The difference between the ionic radii of high-spin iron(III) and cadmium is about 28% ($r_{Cd(II)}$ = 109 pm, $r_{Fe(III)}$ = 78.5 pm [16]). These radii make it very unlikely to assume the formation of simple substitution mixed crystals, but the zeolitic structure of hcfs with its three different kinds of metal ions allows the system much more degrees of freedom for finding a stable lattice. Electrochemical studies, measurements of magnetic susceptibility, X-ray powder diffraction studies, electron spin resonance (ESR), Mössbauer and diffuse reflectance spectroscopy of a wide range of chemically synthesised coprecipitates allow us to obtain a consistent picture of the rather complex processes which lead to the formation of different insertion and substitution mixed phases. The results could be unambiguously interpreted on the basis of a full chemical analysis of all samples. This could never have been possible with the tiny amounts of electrochemically plated films which have been studied in the past.

Experimental

Preparation of samples

All chemical operations were carried out using bidistilled deionised water and analytical or reagent grade chemicals. Prussian blue was prepared as described elsewhere [11]. Preparation of cadmium hexacyanoferrate (II) and -(III) was performed according to literature procedures [24] by adding a $CdSO_4$ solution to a solution of $K_4[Fe(CN)_6]$ and $K_3[Fe(CN)_6]$, respectively. Mixed cadmium-iron(III) hexacyanoferrates were prepared by mixing stoichiometric amounts of $CdSO_4$ and $FeCl_3{\cdot}6H_2O$ or $Fe_2(SO_4)_3$ with $K_4[Fe(CN)_6]$. The precipitate was filtered off and washed with water. The solid was then dried for 15 h in vacuum (0.1 mbar) at ambient temperature and later stored under air.

Chemical analysis

The iron, cadmium and potassium content of all samples was determined by atomic absorption spectrometry of the digested samples. Digestion was achieved by boiling with sulfuric acid. The carbon, nitrogen and hydrogen content was determined by CHN analysis.

Voltammetry

Twice distilled ion-exchanged water and KNO_3 of chemical-grade purity (Merck, Germany) were used for the preparation of the

electrolyte solutions. The reference electrode was Ag/AgCl (3 M KCl, E = 0.208 V vs. SHE at 25 °C) and the auxiliary electrode was a platinum sheet. Voltammetric experiments were performed at 20 ± 2 °C with an AUTOLAB (Eco-Chemie, Utrecht, The Netherlands) and GPES 3.3 software (Eco-Chemie) on a 486 personal computer. All solutions were deoxygenated with high-purity nitrogen for 15 min prior to electrochemical measurements. In this study, the working electrode was a paraffin-impregnated graphite rod (VEB Elektrokohle Lichtenberg, former GDR). The preparation of the electrode is described elsewhere [18]. If not specified otherwise, an aqueous solution of 0.1 M KNO_3 was used as the supporting electrolyte. The voltammograms were recorded with a scan rate of 0.1 V/s, if not specified otherwise.

Magnetic measurements and ESR spectroscopy

A Gouy balance with horizontal hanging of the sample was used for the magnetic susceptibility measurements. Water and a $NiCl_2$ solution (3.51% and 19.52%) served as standards for the calibration. The specific susceptibility of aqueous $NiCl_2$ solution at 20 °C was calculated with the following equation $\chi = [10034p/T - 0.720(1 - p)] \times 10^{-6}$, where p is the weight percentage of $NiCl_2$ and T is the absolute temperature [25]. The instrument used for ESR spectroscopy was a ERS 300 (ZWG, Berlin-Adlershof, Germany).

X-ray powder analysis

A Philips APD 1700 Diffractometer with increments of 0.02° was used to obtain X-ray diffractograms. The time of accumulation was 1 s in the range of 20–80°. Cu-K_α radiation was used and silicon served as an internal standard.

Mössbauer spectroscopy

The samples (15–50 mg/mm^2) were measured in transmission geometry using a Co-57 source of 1 Gbq in a Cr matrix. The spectra were registered with a CM2201 Mössbauer spectrometer (Nauc Pribor, St. Petersburg, Russia) at room temperature by the aid of an iron resonance detector and at liquid nitrogen temperature with a proportional counter.

Parameter fits (Table 1) were performed using a standard least-squares fitting routine. Under the assumption that the f-factors were equal for different iron sites and phases, the subspectra areas were evaluated as a percentage of the total spectrum. The isomer shift was related to metallic iron. Errors for isomer shift, quadrupole splitting and line width were 0.01 mm/s, and for most of the areas it was below 2%; however, for some phases of low concentration it was up to 25% of the obtained area.

Diffuse reflectance spectroscopy

The spectrometer was a transputer integrated diode array system (TIDAS) (J&M Analytische Mess- und Regeltechnik, Germany) with a spectral range from 320 to 950 nm. The number of photo diodes was 256 and the resolution was 3.2 nm/pixel. The spectrometer was interfaced to a personal computer. Powder measurements were performed under a Leitz Laborlux 12 POL S incident light microscope (Leica Mikroskopie und Systeme, Germany) with a 100 W halogen incandescent lamp for illumination. Preliminary studies have shown that the used ${}_0R_0$ geometry allows to use the Kubelka-Munk function F_{KM} as there is direct proportionality between F_{KM} and the concentration of Prussian blue in MgO diluted samples [26]. For calculating the Kubelka-Munk function for the mixed cadmium-iron hexacyanoferrates, the samples were diluted with magnesium oxide in the ratio m_{hcf}/m_{MgO} = 1:50.

Results and discussion

X-ray and Mössbauer spectroscopy

From the ionic radii of cadmium and high-spin iron(III), one cannot expect to find substitution mixed phases. However, the data of the X-ray powder diffraction analysis of the samples showed that the coprecipitates consist of single phases (Table 2). Samples with a molar ratio $m_{Cd} = n_{Cd}/(n_{Cd} + n_{Fe_{hs}})$ smaller than 0.4 have a cubic structure while those with higher ratios are orthorhombic. There is no indication that the samples contain any appreciable amounts of amorphous compounds. It is the most important observation from the X-ray diffraction pattern that during coprecipitation no phase mixture is formed but a single phase of obviously very complex composition. Unfortunately, all precipitates are microcrystalline and no crystals of a sufficient size were accessible to perform a single-crystal X-ray fine structure analysis. The parameters of the Mössbauer spectra (Table 2) indicate that high-spin iron ions are substituted by cadmium ions. This substitution leads to a change in the ratio of the amount of low-spin iron to the amount of high-spin iron and also to a shift of both signals owing to a change in the chemical environment of both types of iron ions. The substitution is accompanied by an increase in the chemical shift δ of both iron ions. This is a clear indication of a decreasing covalency of the metal-ligand bond occurring during the substitution of Fe^{III}_{hs} by Cd^{II}. A similar effect is well known from hcfs(II): increasing ionic radii of the N-coordinated metal ions of hcfs are accompanied by a decrease in the covalency of the iron-cyanide bond [27]. An important result of Mössbauer measurements is that they give evidence of the presence of high-spin iron(II) in some of the precipitates. The Fe^{II}_{hs} state appears as a line at 1.85 mm (see Fig. 1). Such a signal has never been observed for samples where m_{Cd} is smaller than 0.4. This also implies that the Fe^{II} cannot be an impurity from synthesis.

Chemical analysis and derived structure models

By chemical analysis of the Fe (Fe_{ls} and Fe_{hs}), Cd, K, C, N and H content the molar ratio $m_{Cd} = n_{Cd}/(n_{Cd} + n_{Fe_{hs}})$ and the composition of each sample was calculated (see Table 3). To do so, the first rule was to assume that the hcf units form an ideal sublattice, i.e. all α positions (Fig. 2) are occupied by low-spin iron ions. This means that per formula unit there is exactly one hcf ion. This is reasonable because it is supported by all previous results reported in literature with the only exception of a Prussian blue which was extremely slowly crystallised from hydrochloric acid and which did not contain potassium ions for stabilising the structure [28]. The calculated data are shown in Table 3 (column 1). It can be seen from these data that the balance of the

Table 1 Simulation data of Mössbauer spectra of the samples shown in Fig. 1

Multiplet	Parameter	Value	± Delta
Sample M1 (m_{Cd} = 1.000)			
Base line	Intensity	1104230.8912397	73.4237014
Doublet 1	Isomer shift (mm/s)	−0.1016783	0.0001664
	Half width (mm/s)	0.2265296	0.0011233
	Signal area (%)	96.3864083	0.2062872
	Quadrupole split (mm/s)	0.0814826	0.0013416
	Area ratio re/li	1.0000000	Fixed parameter
Doublet 2	Isomer shift (mm/s)	1.2387277	0.1121653
	Half width (mm/s)	1.5179398	0.3216851
	Signal area (%)	3.6135917	0.8308417
	Quadrupole split (mm/s)	2.3933088	0.2023642
	Area ratio re/li	1.0000000	Fixed parameter
Sum of square error: 1056.237, Chi-square: 1.025094, Line shape: 28.000% Gauss			
Sample M2 (m_{Cd} = 0.478)			
Base line	Intensity	3778425.5007220	129.4447106
Doublet 1	Isomer shift (mm/s)	−0.1019991	0.0001614
	Half width (mm/s)	0.2326679	0.0011398
	Signal area (%)	84.4309481	0.2124921
	Quadrupole split (mm/s)	0.1059849	0.0006359
	Area ratio re/li	1.0000000	Fixed parameter
Doublet 2	Isomer shift (mm/s)	0.8076338	0.0035311
	Half width (mm/s)	0.2315673	0.0090427
	Signal area (%)	3.5601459	0.1401971
	Quadrupole split (mm/s)	2.1349174	0.0070739
	Area ratio re/li	1.0000000	Fixed parameter
Doublet 3	Isomer shift (mm/s)	0.4469932	0.0097144
	Half width (mm/s)	0.9660138	0.0689395
	Signal area (%)	12.0089060	0.4471675
	Quadrupole split (mm/s)	0.0063438	0.2574324
	Area ratio re/li	1.0000000	Fixed parameter
Sum of square error: 2182.892, Chi-square: 1.290460, Line shape: 13.000% Gauss			
Sample M3 (m_{Cd} = 0.870)			
Base line	Intensity	3674454.5943026	114.2198311
Doublet 1	Isomer shift (mm/s)	−0.1192120	0.0003124
	Half width (mm/s)	0.2279522	0.0011042
	Signal area (%)	62.1866680	0.3907395
	Quadrupole split (mm/s)	0.1270888	0.0006352
	Area ratio re/li	1.0000000	Fixed parameter
Doublet 2	Isomer shift (mm/s)	0.9546054	0.0153842
	Half width (mm/s)	0.3966448	0.0167524
	Signal area (%)	6.1637845	0.2160161
	Quadrupole split (mm/s)	1.8119040	0.0312031
	Area ratio re/li	1.0000000	Fixed parameter
Doublet 3	Isomer shift (mm/s)	0.4466685	0.0043988
	Half width (mm/s)	0.4629216	0.0063500
	Signal area (%)	31.6495476	0.5048128
	Quadrupole split (mm/s)	0.3236867	0.0043763
	Area ratio re/li	1.0000000	Fixed parameter
Sum of square error: 2451.970, Chi-square: 1.683628, Line shape: 25.000% Gauss			

charges of the anions $[Fe(CN)_6]^{4-}$ and the cations (K^{I} + Cd^{II} + Fe^{III}) seems to be preserved only in the range of $0 \le m_{Cd} < 0.4$. For $m_{Cd} > 0.4$, a deficit of positive charges is observed in the formulas. This may mean that a partial oxidation of the low-spin iron occurs according to: $Fe^{II}_{ls} \rightarrow (1-y)Fe^{II}_{ls} + yFe^{III}_{ls}$. This oxidation is accompanied by a reconstruction of the unit cell and also by the appearance of Fe^{II}_{hs} ions (see Table 2). In order to calculate a possible distribution of cations in the channels and in the lattice framework, a model was used in which the three-dimensional cubic lattice is constructed of $[Fe^{II}(CN)_6M^{n+}]^{(4-n)-}$ units [27, 29]. All remaining cations are located in the channels and provide the overall charge balance. The rigid framework of the lattice of the samples can be represented by the formula $[Fe^{II}_{1-y}Fe^{III}_{y}(CN)_6Cd^{II}_{z}Fe^{III}_{1-z}]^{(y+z)-}$. In this formula, the cations on the left side of the cyanide ions are those which are coordinated to the carbon (Fe^{II}_{ls}, Fe^{III}_{ls}). The ions on the right side of CN are those coordinated to the nitrogen (see Fig. 2). The remaining potassium ions and Fe^{III}_{hs} or Cd^{II} ions are located in the channels $\{K_kCd_jFe_m \cdot nH_2O\}^{(y+z)+}$. The next assumption was that cadmium ions can substitute the high-spin iron ions at their nitrogen-coordinated sites only when their concentration exceeds that which can be found in the interstitials. The formulas in column 2 of Table 3 are

Table 2 Data of X-ray diffraction and Mössbauer spectrocopy measurements ($T = R$, $v = 30$)

m_{Cd} [a]	X-ray diffraction data				Mössbauer spectrocopy data					
	Symmetry	a (Å)	b (Å)	c (Å)	Fe_{ls}^{2+}		Fe_{hs}^{3+}		Fe_{hs}^{2+}	
					δ	%	δ	%	δ	%
0.000	cub.	10.20	–	–	−0.152	43.50	0.387	56.50	–	–
9×10^{-4}	cub.	10.20	–	–	–	–	–	–	–	–
0.036	cub.	10.22	–	–	–	–	–	–	–	–
0.086	cub.	10.24	–	–	–	–	–	–	–	–
0.126	cub.	10.26	–	–	–	–	–	–	–	–
0.200	cub.	10.34	–	–	–	–	–	–	–	–
0.374	cub.	10.48	–	–	−0.126	58.42	0.408	41.58	–	–
0.478	orth.	–	–	–	−0.119	62.19	0.444	31.65	0.954	6.16
0.569	orth.	–	–	–	–	–	–	–	–	–
0.694	orth.	–	–	–	−0.115	69.41	0.447	24.46	0.915	6.13
0.821	orth.	–	–	–	–	–	–	–	–	–
0.870	orth.	–	–	–	−0.102	84.43	0.447	12.01	0.807	3.56
0.938	orth.	10.43	10.21	9.82	−0.101	91.18	0.589	3.16	0.975	5.66
1.000[b]	orth.	10.45	10.24	9.94	−0.102	96.39	–	–	1.239	3.61
1.000[c]	cub.	10.66	–	–	−0.109[d] Fe_{ls}^{3+}	80.8[d] Fe_{ls}^{3+}	–	–	–	–
					−0.107[d] Fe_{ls}^{2+}	19.2[d] Fe_{ls}^{2+}				

[a] This is the molar ratio of Cd^{2+} in the samples according to chemical analysis: $m_{Cd} = n_{Cd}/(n_{Cd} + n_{Fe_{hs}})$
[b] Synthesised with $K_4[Fe(CN)_6]$
[c] Synthesised with $K_3[Fe(CN)_6]$
[d] $T = R$, $v = 10$

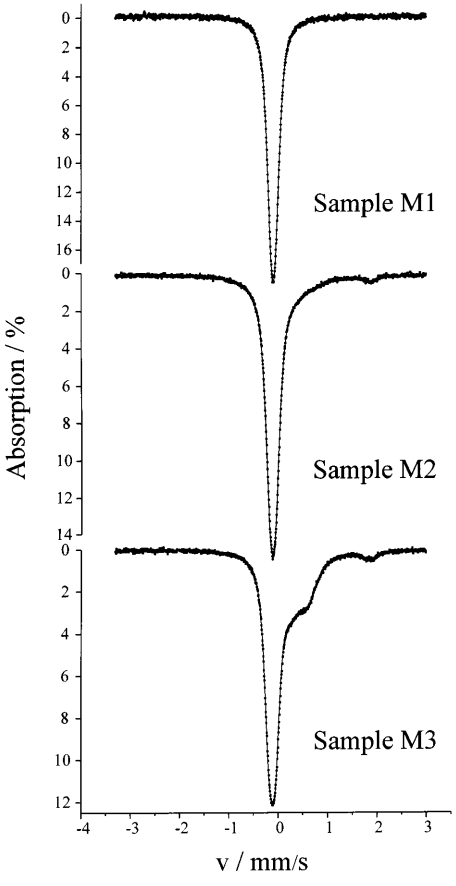

Fig. 1 Mössbauer spectra: *sample M1* pure cadmium hexacyanoferrate(II), $m_{Cd} = 1.000$ (synthesised with $K_4[Fe(CN)_6]$); *sample M2* mixed cadmium-iron(III) hexacyanoferrate(II), $m_{Cd} = 0.478$; *sample M3* mixed cadmium-iron(III) hexacyanoferrate(II), $m_{Cd} = 0.870$, where the dots show the measured spectra and the lines represent the simulated curves derived from the data of Table 1

based upon the chemical analysis of the constituting elements. The distribution to the different positions (see Fig. 2) and to the valence states was realised in such way that the charge balance could be maintained. This was only unambiguously possible by sticking to the above outlined assumptions. Hence these formulas remain to some extend hypothetical, but it will be shown that they provide a consistent explanation of the experimental results.

From Fig. 2, it follows that three different kinds of mixed crystals are possible:

1. Insertion mixed crystals: position γ is randomly populated by different cations.
2. Substitution mixed crystals: position β is randomly populated by different cations.
3. Valency mixed crystals: (a) position α is randomly populated by Fe_{ls}^{II} and Fe_{ls}^{III}; (b) iron ions at position β are randomly distributed, being Fe_{hs}^{III} and Fe_{hs}^{II}; (c) iron ions at position γ are randomly distributed, being Fe_{hs}^{III} and Fe_{hs}^{II}.

The real situation can become, in principle, even more complicated by the simultaneous formation of different kinds of mixed crystals. The formation of insertion-mixed crystals at low cadmium content, which will be accompanied by an elongation of the lattice parameters, allows the formation of substitution-mixed crystals at higher cadmium content. When the cadmium content is sufficiently high, all the nitrogen coordination sites are taken by these ions and a possible excess amount goes to the interstitial sites. Based on these principal assumptions, the composition of the different coprecipitates was calculated. The results of this computation are shown in Table 3, column 2. On the basis of the Mössbauer spec-

Table 3 Chemical composition of the $(Fe_{1-x}Cd_x)[Fe(CN)_6]$ samples

m_{Cd} [a]	Column 1 Formula (mass balance only)	Column 2 Formula (mass and charge balance)[d]
0.000	$\{K_{0.16}Fe_{1.28}3.0H_2O\}^{4+}[Fe(CN)_6]$	$\{K_{0.16}Fe^{III}_{0.28}3.0H_2O\}[Fe^{II}_{1.00}(CN)_6Fe^{III}_{1.00}]$
9×10^{-4}	$\{K_{0.70}Cd_{0.001}Fe_{1.10}3.1H_2O\}^{4+}[Fe(CN)_6]$	$\{K_{0.70}Cd_{0.001}Fe^{III}_{0.10}3.1H_2O\}[Fe^{II}_{1.00}(CN)_6Fe^{III}_{1.00}]$
0.036	$\{K_{0.68}Cd_{0.04}Fe_{1.08}3.0H_2O\}^{4+}[Fe(CN)_6]$	$\{K_{0.68}Cd_{0.04}Fe^{III}_{0.08}3.0H_2O\}[Fe^{II}_{1.00}(CN)_6Fe^{III}_{1.00}]$
0.086	$\{K_{0.62}Cd_{0.10}Fe_{1.06}2.9H_2O\}^{4+}[Fe(CN)_6]$	$\{K_{0.62}Cd_{0.10}Fe^{III}_{0.06}2.9H_2O\}[Fe^{II}_{1.00}(CN)_6Fe^{III}_{1.00}]$
0.126	$\{K_{0.58}Cd_{0.15}Fe_{1.04}3.0H_2O\}^{4+}[Fe(CN)_6]$	$\{K_{0.58}Cd_{0.15}Fe^{III}_{0.04}3.0H_2O\}[Fe^{II}_{1.00}(CN)_6Fe^{III}_{1.00}]$
0.200	$\{K_{0.78}Cd_{0.23}Fe_{0.92}3.0H_2O\}^{4+}[Fe(CN)_6]$	$\{K_{0.78}Cd_{0.15}3.0H_2O\}[Fe^{II}_{1.00}(CN)_6Fe^{III}_{0.92}Cd_{0.08}]$
0.374	$\{K_{0.98}Cd_{0.43}Fe_{0.72}2.9H_2O\}^{4+}[Fe(CN)_6]$	$\{K_{0.98}Cd_{0.15}2.9H_2O\}[Fe^{II}_{1.00}(CN)_6Fe^{III}_{0.72}Cd_{0.28}]$
0.478	$\{K_{1.03}Cd_{0.54}Fe_{0.59}2.7H_2O\}^{3.88+}[Fe(CN)_6]$	$\{K_{1.03}Fe^{III}_{0.13}2.7H_2O\}[Fe^{II}_{0.78}Fe^{III}_{0.22}(CN)_6Fe^{III}_{0.36}Fe^{II}_{0.10}Cd_{0.54}]$
0.569	$\{K_{1.17}Cd_{0.62}Fe_{0.47}1.8H_2O\}^{3.82+}[Fe(CN)_6]$	$\{K_{1.17}Fe^{III}_{0.09}1.8H_2O\}[Fe^{II}_{0.73}Fe^{III}_{0.27}(CN)_6Fe^{III}_{0.29}Fe^{II}_{0.09}Cd_{0.62}]$
0.694	$\{K_{1.33}Cd_{0.75}Fe_{0.33}1.8H_2O\}^{3.82+}[Fe(CN)_6]$	$\{K_{1.33}Fe^{III}_{0.08}1.8H_2O\}[Fe^{II}_{0.74}Fe^{III}_{0.26}(CN)_6Fe^{III}_{0.17}Fe^{II}_{0.08}Cd_{0.75}]$
0.821	$\{K_{1.38}Cd_{0.92}Fe_{0.20}1.9H_2O\}^{3.82+}[Fe(CN)_6]$	$\{K_{1.38}Fe^{III}_{0.12}1.9H_2O\}[Fe^{II}_{0.75}Fe^{III}_{0.25}(CN)_6Fe^{II}_{0.08}Cd_{0.92}]$
0.870	$\{K_{1.37}Cd_{1.00}Fe_{0.15}1.9H_2O\}^{3.82+}[Fe(CN)_6]$	$\{K_{1.37}Fe^{III}_{0.08}Fe^{II}_{0.07}1.9H_2O\}[Fe^{II}_{0.75}Fe^{III}_{0.25}(CN)_6Cd_{1.00}]$
0.938	$\{K_{1.51}Cd_{1.05}Fe_{0.07}1.9H_2O\}^{3.82+}[Fe(CN)_6]$	$\{K_{1.51}Fe^{III}_{0.03}Fe^{II}_{0.04}Cd_{0.05}1.9H_2O\}[Fe^{II}_{0.78}Fe^{III}_{0.22}(CN)_6Cd_{1.00}]$
1.000[b]	$\{K_{1.52}Cd_{1.15}1.6H_2O\}^{3.82+}[Fe(CN)_6]$	$\{K_{1.52}Fe^{II}_{0.04}Cd_{0.11}1.6H_2O\}[Fe^{II}_{0.82}Fe^{III}_{0.18}(CN)_6Cd_{1.00}]$
1.000[c]	$\{K_{0.14}Cd_{1.49}3.0H_2O\}^{3.12+}[Fe(CN)_6]$	$\{K_{0.14}Cd_{0.49}3.0H_2O\}[Fe^{III}_{0.88}Fe^{II}_{0.12}(CN)_6Cd_{1.00}]$

[a] This is the molar ratio of Cd^{2+} in the samples according to chemical analysis: $m_{Cd} = n_{Cd}/(n_{Cd} + n_{Fe_{hs}})$
[b] Synthesised with $K_4[Fe(CN)_6]$
[c] Synthesised with $K_3[Fe(CN)_6]$
[d] Calculated based on the model explained in the text

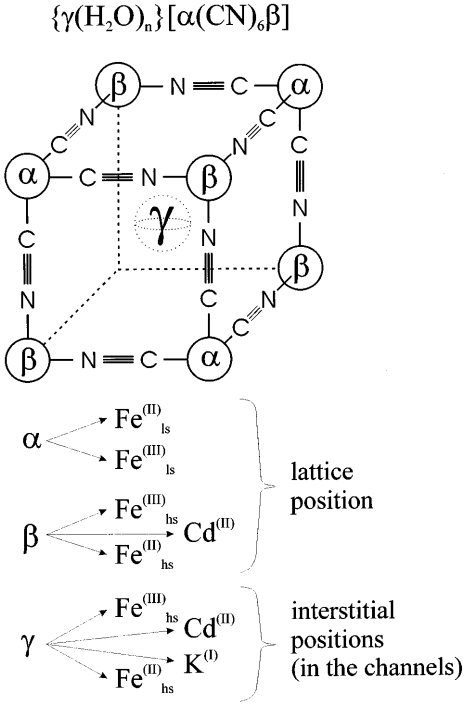

Fig. 2 The structure of solid Prussian blue and of mixed iron-cadmium hexacyanoferrates (hcfs) with possible occupation of different sites by K^+, Cd^{2+} and Fe^{3+}

troscopy data, we introduced 6% Fe^{II}_{hs} of the total amount of high-spin iron for the samples with $m_{Cd} > 0.4$. The following features can be derived from this table:

1. Very small amounts of Cd^{II} ions (e.g. 9×10^{-4} mol/formula unit), when located in the channels (γ position) of Prussian blue, induce a reconstruction of the nearly 'insoluble' Prussian blue $K_{0.16}Fe_{1.28}[Fe(CN)_6]$ into nearly "soluble" Prussian blue $K_{0.70}Fe_{1.10}[Fe(CN)_6]$ with a remarkable increase of potassium ion concentration in the channels.
2. In the range of $9 \times 10^{-4} < m_{Cd} < 0.126$, the composition of the framework lattice $[Fe^{II}(CN)_6Fe^{III}]^-$ and the content of K^I ions in the channels remains almost constant. Cd^{II} ions and Fe^{III} ions are also situated in the channels. The samples can be described by an f-centred cubic unit cell with $a = 10.20$ Å. The value of the a parameter agrees with the one for $K_{0.25}Fe_{1.25}[Fe(CN)_6]$ [30]. The authors of [28] calculated this parameter as 10.18 Å for $Fe_4[Fe(CN)_6]_3$. With decreasing Fe^{III} content, the Cd^{II} ions substitute Fe^{III}_{hs} ions in the channels and the a parameter begins to increase (see Table 2).
3. For $m_{Cd} > 0.126$, the amount of Fe^{III}_{hs} decreases below 1.0 mol/formula unit. There is a lack of Fe^{III}_{hs} ions to fill the β position of the framework lattice. This deficit is filled up by Cd^{II} ions. These phases still maintain a cubic structure but the lattice parameter increases and reaches 10.34 Å and 10.48 Å for the samples with $m_{Cd} = 0.200$ and 0.374, respectively. In the range of $0 \le m_{Cd} \le 0.374$, the amount of cations in the channels suffices for the complete compensation of the negative charge in the framework unit cell.
4. When m_{Cd} reaches 0.478, the balance of charges cannot be maintained on the basis of the chemical synthesis and the starting oxidation states of iron (see Table 3, column 1). This situation requires the introduction of a certain amount of Fe^{III}_{ls} in the α positions. Indeed, starting at $m_{Cd} = 0.478$, the Mössbauer spectra (Fig. 1) show the response of Fe^{II}_{hs} ions. The samples have primitive orthorhombic unit

cells with the following parameters: a = 10.45 Å, b = 10.24 Å and c = 9.94 Å for the sample with m_{Cd} = 1.000 (synthesised with $K_4[Fe(CN)_6]$). These parameters are not much different from those of the phase $K_2[Fe(CN)_6Cd]$ [31]. For the samples with m_{Cd} in the range of $0.478 \le m_{Cd} \le 0.870$, the parameters of the crystal lattice are not given because of a considerable experimental error in their determination. The composition of Cd hcf(III) (synthesised with $K_3[Fe(CN)_6]$) requires the presence of 12% Fe^{II}_{ls} to maintain the charge balance. The resolution of Mössbauer spectra of such a phase on two groups of lines showed that another form of Fe_{ls} is involved at a content of 19% (see Table 2). In contrast to Cd hexacyanoferrate(II), this phase is described by an f-centred cubic unit cell with a = 10.66 Å.

It is necessary to pay attention to the effect of crystal water. One mole of the sample with cubic symmetry contains about three moles of water, while one mole of a sample with orthorhombic symmetry does not contain more than two moles of water. It is possible that this effect is due to the content of potassium cations. For example, it has been observed [32] that an increasing amount of alkali cations in the metal hcfs is accompanied by a loss of water. In the present system, one mole of the cubic phase contains less than one mole of K^+ whereas the orthorhombic samples have more than one mole of K^+ per mole of hcf. The samples shown in Table 3 can be divided into three groups:

1. First group ($0 \le m_{Cd} \le 0.126$): all physico-chemical properties are practically identical with Prussian blue.
2. Second group ($0.2 \le m_{Cd} \le 0.478$): the samples have properties of mixed phases but they have still strong similarities with Prussian blue.
3. Third group ($0.569 \le m_{Cd} \le 1.0$): the samples have properties of mixed phases but they are more related to those of cadmium hcf(II).

Figure 3 shows the distribution of the cations and the water in the channels as a function of m_{Cd}. Of course, one has to bear in mind that the very insoluble hcfs exhibit a tendency to form compounds with variable composition, including phases with appreciable concentrations of defects, e.g. missing hcf units. Thus, the formulas in Table 3 might be oversimplified, but it is striking that all experimental results can be explained on their basis.

Solid state electrochemistry (voltammetry of immobilised microparticles)

Typical cyclic voltammograms of cadmium hcf(III) and -(II) are shown in Figs. 4 and 5. The voltammograms of Cd hcf(II) in Fig. 4b are those of a freshly synthesised sample. Figure 5a shows the voltammograms of a one-month-old sample. Cadmium hcf(III) exhibits reversible electrochemistry in cyclic voltammetry (see Figs. 4a and 5c). The first and all following cyclic voltammograms are almost of the same shape and appear at the same potentials. However, cadmium hcf(II) shows a different behaviour in the first oxidation half-cycle. As Figs. 4b and 5a show, the oxidation peak appears in the first cycle at a much more positive potential and a small shoulder is visible just at that place where in the following cycles the oxidation peak is situated. The latter peak is also identical with the oxidation peak of cadmium hcf(III). It is very important to note that upon storing the cadmium hcf(II), especially when light is not excluded, the shoulder grows to become a distinct peak

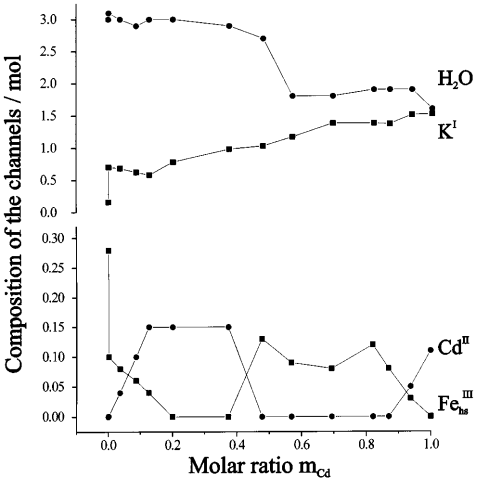

Fig. 3 Plot of the composition of the channels as a function of the molar ratio m_{Cd} of the ($Fe_{1-x}Cd_x$) hcf(II) samples

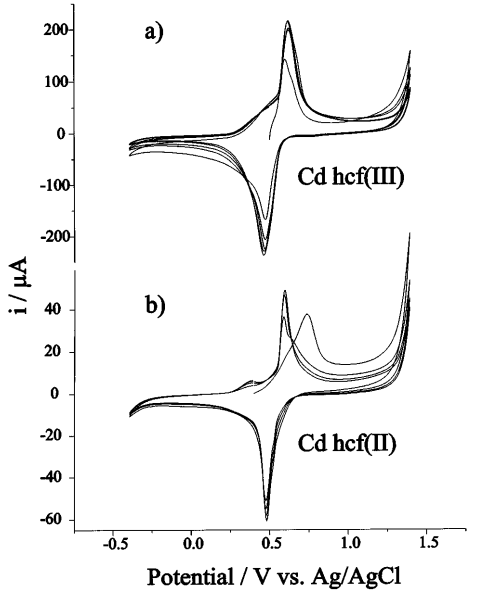

Fig. 4 Typical cyclic voltammograms of **a** cadmium hcf(III), m_{Cd} = 1.000 (synthesised with $K_3[Fe(CN)_6]$), **b** freshly synthesised cadmium hcf(II), m_{Cd} = 1.000 (synthesised with $K_4[Fe(CN)_6]$) (start potential 0.4 V)

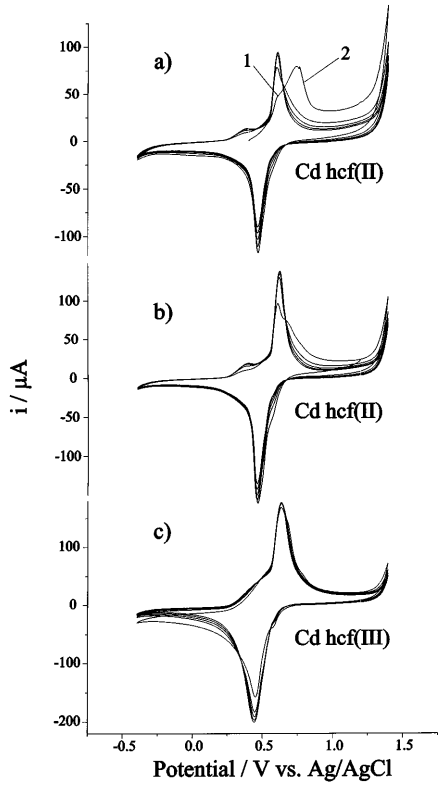

Fig. 5 Typical cyclic voltammograms of **a** cadmium hcf(II), 1 month after production, start potential 0.4 V, **b** freshly synthesised cadmium hcf(II), start potential 1.2 V and **c** cadmium hcf(III), start potential 1.2 V

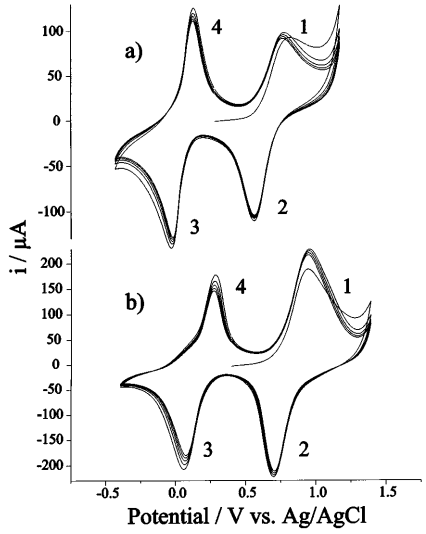

Fig. 6 Typical cyclic voltammograms of **a** pure Prussian blue, m_{Cd} = 0.000 and **b** mixed iron(III)-cadmium hcf(II), m_{Cd} = 0.001 (start potential 0.4 V)

(see Figs. 4b and 5a); when the start potential is more positive than 0.9 V (Fig. 5b), the behaviour of cadmium hcf(II) is almost identical with that of cadmium hcf(III) (Figs. 4a, 5c).

The chemical analysis (see Table 3) shows that the Cd hcf(III) contains almost five times more Cd^{2+} in the channels than Cd hcf(II)

It is known that the formal potential of Cd hcf(II/III) is more positive in a Cd^{2+} solution than in a K^+ solution. Obviously, a slow chemical oxidation also occurs upon storing Cd hcf(II), especially when light is not excluded. This chemical oxidation, presumably by oxygen, will also be accompanied by a release of Cd^{2+} ions which may collect at the surface of the Cd hcf in the form of cadmium hydroxide. That is seen in the CV of aged Cd hcf(II) in Fig. 5a as an increase of the signal 1 appearing as a well-developed shoulder of signal 2.

The cyclic voltammograms of pure Prussian blue (m_{Cd} = 0.000) and iron-cadmium hcf(II) ($m_{Cd} = 9 \times 10^{-4}$) show (Fig. 6) that a small amount of cadmium ions causes an increase of the response of the pair $Fe_{ls}^{III/II}$ (signals 1 and 2) as compared to that of $Fe_{hs}^{II/III}$. Therefore, the ratio R of the peak current 1 (I_1) to the peak current 3 (I_3) or to the peak current 4 (I_4) increases nearly twice for the sample with $m_{Cd} = 9 \times 10^{-4}$ (curve b) as compared to a pure Prussian blue sample (curve a). The increase in the intensity of the Fe_{ls} signal as compared to the Fe_{hs} signal finds an easy explanation in the analytical data (Table 3), which show that upon introduction of Cd^{2+} ($m_{Cd} = 9 \times 10^{-4}$) there occurs a drop in Fe_{hs} concentration of almost 20%. The dependences of $R(I_1/I_3)$ and $R(I_1/I_4)$ on m_{Cd} (Fig. 7, curves 1 and 2) show that there are three distinct parts, the borders of which coincide with the introduction of iron or cadmium ions into new positions as implied in the formulas in Table 3. The shape of these plots exactly follows that of the ratio of $Fe_{ls}^{II}/Fe_{hs}^{III}$ (curve 3) as calculated from Table 3, and it is very similar to the plot of K^+ concentration versus m_{Cd} (Fig. 3, curve 3). In accordance with the data from X-ray and Mössbauer spectroscopy, the electrochemistry also shows that the chemically synthesised samples of cadmium-iron(III) hcf(II) are not mixtures of phases but members of a series of substitution mixed phases. As Fig. 8 shows, the first scan of the voltammograms of a mechanical mixture of iron(III) hcf(II) with freshly synthesised cadmium hcf(II) (ratio 1: 1) has two distinct peaks of Fe_{ls}^{II} oxidation (curve a). The formal potentials of $Fe_{hs}^{II/III}$ and $Fe_{hs}^{III/II}$ pairs do not depend on the ratio of cadmium hcf(II) to iron(III) hcf(II) (Fig. 9, curves 1 and 2). For the chemically synthesised iron(III) cadmium hcf(II) with the same $Cd^{II} : Fe_{hs}^{III}$ ratio (curve b), a single peak of Fe_{ls}^{II} oxidation is observed in the first cycle (Fig. 8b). The shape of this peak current does not change with the increase of m_{Cd} but the peak potential shifts to more positive values (Fig. 8c). The shape of the plots of the formal potentials of $Fe_{hs}^{III/II}$ and $Fe_{hs}^{III/II}$ pairs (Fig. 9, curves 3 and 4, respectively) versus m_{Cd} indicates the formation of a continuous series of the substitution mixed phases. Whereas the formal potentials of the two iron systems are independent of the composition of the powder mixtures, the plots of $E_f = f(m_{Cd})$ have three

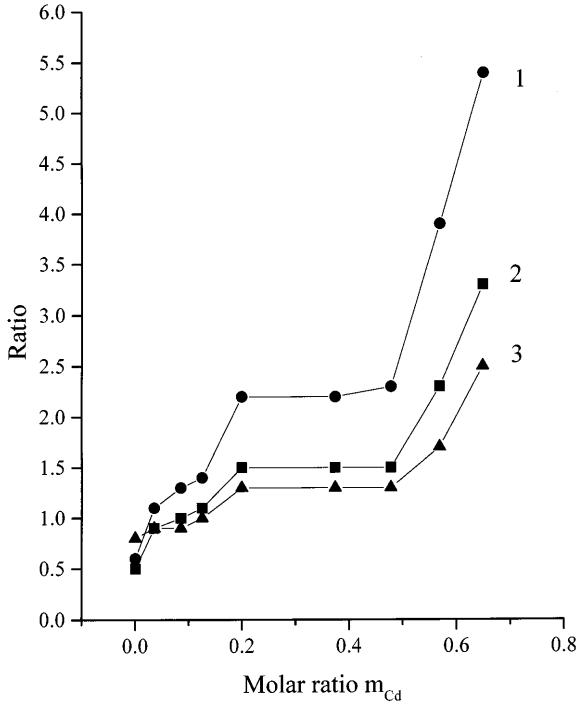

Fig. 7 Plot of the ratios of *1* I_1/I_4, *2* I_1/I_3 (I_1, I_3, I_4 see Fig. 6) and *3* $Fe^{II}_{ls}/Fe^{III}_{hs}$ as a function of the molar ratio m_{Cd} of the $(Fe_{1-x}Cd_x)$ hcf(II) samples. The ratio of $Fe^{II}_{ls}/Fe^{III}_{hs}$ has been calculated from Table 3

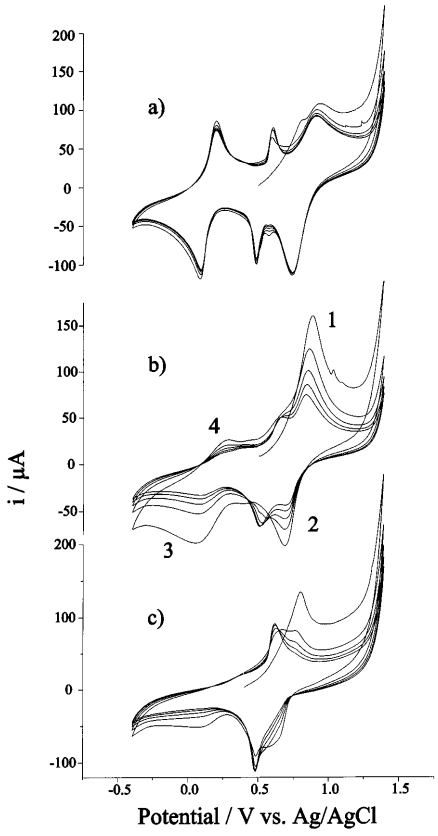

Fig. 8 Typical cyclic voltammograms of **a** a mechanical mixture of iron(III) hcf(II) and freshly synthesised cadmium hcf(II) in the ratio 1 : 1, **b** chemically synthesised mixed cadmium-iron(III) hcf(II) with m_{Cd} = 0.478 and **c** chemically synthesised mixed cadmium-iron(III) hcf(II) with m_{Cd} = 0.821 (start potential −0.4 V)

distinct parts for the case of coprecipitates, the borders of which coincide with the introduction of iron or cadmium ions into new positions as was assumed in the calculations for Table 3. In the range of $0 \le m_{Cd} \le 0.126$ when the parameter a of the cubic crystal lattice is constant (see Table 2), the formal potential of the $Fe^{III/II}_{ls}$ pair of the mixed phases $(Fe_{1-x}Cd_x)[Fe(CN)_6]$ does not differ from that of the pure Prussian blue ($\Delta E_f/\Delta m_{Cd} = 0$). When cadmium ions start to substitute the Fe^{III}_{hs} ions in the lattice (β position in Fig. 2, the range of $0.126 \le m_{Cd} \le 0.478$ in Table 3), the formal potential of the $Fe^{III/II}_{ls}$ pair shifts to more negative values ($\Delta E_f/\Delta m_{Cd}$ = 100 mV/mol). Although the symmetry of the crystals remains cubic, the lattice constant increases. The plot of $E_f = f(m_{Cd})$ has the largest slope ($\Delta E_f/\Delta m_{Cd}$ = 420 mV/mol) for $Fe^{III/II}_{ls}$ when the symmetry of the crystal structure is changing and when the properties of the samples approach those of cadmium hcf(II). It is obvious that for the coprecipitated samples the plot of $E_f = f(m_{Cd})$ of the $Fe^{III/II}_{hs}$ pair is related to the composition of the channels. The formal potential shifts to more positive positions until the Fe^{III}_{hs} ions are situated in the channels and the formal potential is constant when K^+ and Cd^{2+} ions completely occupy the channels (see Fig. 3 and Fig. 9, curve 4).

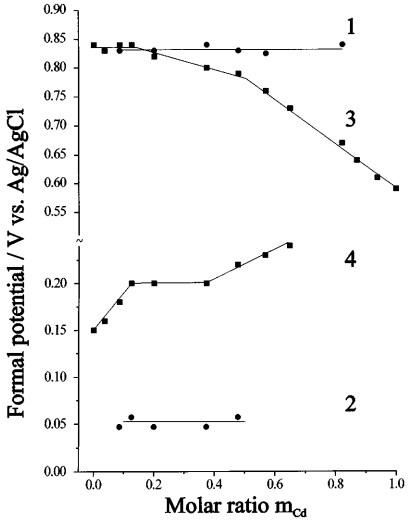

Fig. 9 Plot of the formal potentials $E_f = (E_c + E_a)/2$: *1* and *2* of the powder mixtures of cadmium hcf(II) and Prussian blue for $Fe^{III/II}_{ls}$ and $Fe^{III/II}_{hs}$ pairs, respectively; *3* and *4* of coprecipitated mixed iron(III)-cadmium hcf(II) for $Fe^{III/II}_{ls}$ and $Fe^{III/II}_{hs}$ pairs, respectively, as a function of molar ratio m_{Cd} of the $(Fe_{1-x}Cd_x)$ hcf(II) samples

Magnetic susceptibility and ESR spectroscopy

The next step in this study was to look whether the proposed formulas and the electrochemical behaviour

can be correlated with the magnetic properties of the samples. The measurements of the magnetic susceptibility showed that all studied samples possess a magnetic moment. The only exception was the sample with $m_{Cd} = 1.000$, which was synthesised using $K_4[Fe(CN)_6]$, that was diamagnetic while the mixed cadmium-iron hcf(II) with $m_{Cd} = 0.938$ was paramagnetic. In accordance with the data in Table 3, it has 0.07 moles of high-spin iron ions per unit of formula. The colour of this sample is light blue whereas pure cadmium hcf(II) is white. The value χ_g of the freshly prepared compound was -4.0×10^{-7} and it increased up to -1.6×10^{-7} during storage at room temperature within one month. Obviously a certain part of the cadmium hcf(II) was oxidised to cadmium hcf(III). One cadmium hcf(III) sample with $m_{Cd} = 1.000$, which was synthesised using $K_3[Fe(CN)_6]$, was paramagnetic ($\chi_g = 3.3 \times 10^{-6}$).

Figure 10 shows how the magnetic susceptibility changes when cadmium is increasingly introduced into Prussian blue (curve a). In the case of the cadmium-iron hcfs studied, possible candidates for paramagnetism are high-spin iron(III), low-spin iron(III) and exchange coupled ions. Based on the formulas given in Table 3, the net contents of ($Fe^{III}_{hs} + Fe^{III}_{ls}$) were calculated and represented in Fig. 10 as curve b. Obviously, the magnetic susceptibility of the samples changes in the same way as the iron(III) content. A comparison with the data of Table 3 reveals that the qualitative steps which the magnetic susceptibility exhibits are caused by changing the nature of substituted iron ions, i.e. interstitial (γ position) or nitrogen-coordinated (β position) iron ions, respectively. Especially remarkable is the fact that the smallest amount of added cadmium, i.e. at $m_{Cd} = 9 \times 10^{-4}$, not only causes a simple substitution of a charge-equivalent amount of interstitial iron(III) ions but initiates an ultimately almost complete substitution of the interstitial iron(III) ions by potassium ions. This drop in the iron(III) concentration in the interstitials can also be deduced from the experimental results of ESR spectroscopy and electrochemistry. It is well known that so-called "soluble" and "insoluble" Prussian blues can be distinguished from each other by their potassium and iron content in the interstitials. The insoluble form bears more iron(III), and the soluble form more potassium ions, at the interstitial positions [33]. This can also be demonstrated on the basis of the ratio of magnetic susceptibilities ($\gamma_{insol}/\gamma_{sol} = 1.15$) which is almost the same as appears as the ratio of the ($Fe^{III}_{hs} + Fe^{III}_{ls}$) quantity for the samples with $m_{Cd} = 0$ and $m_{Cd} = 9 \times 10^{-4}$ $(Fe^{III}_{hs} + Fe^{III}_{ls})_{insol}/(Fe^{III}_{hs} + Fe^{III}_{ls})_{sol} = 1.16$). Indeed, it was observed that the sample with $m_{Cd} = 9 \times 10^{-4}$ exhibits the tendency to form a colloidal solution whereas the sample with $m_{Cd} = 0$ was really the so-called insoluble form of Prussian blue. Just as in the electrochemical experiments, the curve also exhibits three distinct parts, the borders of which coincide with the introduction of iron or cadmium ions into new positions as implied in the formulas in Table 3.

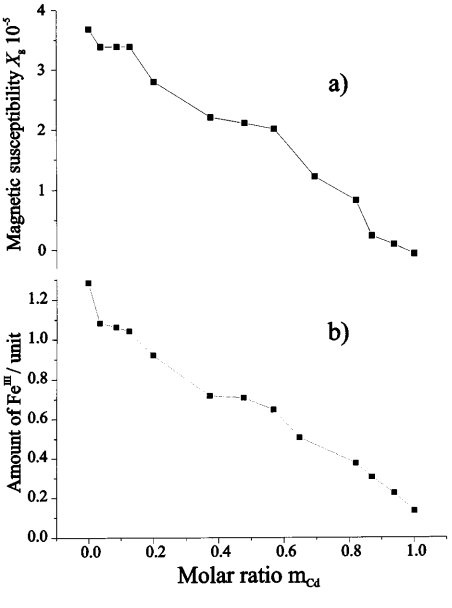

Fig. 10 Plot of **a** the magnetic susceptibility and **b** the amount of $Fe^{III}_{hs} + Fe^{III}_{ls}$ as a function of the molar ratio m_{Cd} of the ($Fe_{1-x}Cd_x$) hcf(II) samples

ESR spectroscopy revealed that in the range from $m_{Cd} = 0$ up to $m_{Cd} = 0.478$ the spectra consist of a single resonance line with a g factor of 2 (see Fig. 11, first six curves on the left side). This indicates a strong crystal field. In the range of $0.478 \le m_{Cd} \le 1.0$ where the orthorhombic crystals are formed, an additional resonance line with an effective g factor of about 4.3 appears in the ESR spectra (signal B in Fig. 11). The intensity of this line increases with increasing x. Signal B indicates the presence of Fe^{III}_{hs} in a less symmetric environment and with less effective exchange interactions. The signal is confined to the range of $0.478 \le m_{Cd} \le 1.0$ in which there will exist subunits of the lattice with only Cd^{2+} at position β surrounding one Fe^{III}_{hs} ion at position γ. Samples with $0.821 \le m_{Cd} \le 0.38$ exhibit the signals C and D, which are well developed at 77 K. The two signals are attributed to axially distorted iron(III) species with an effective g value around 18 [34]. This g value, and the fact that the signals disappear at elevated temperature, allows us to formulate the responsible centres as follows:

$$\{Fe^{III} \cdots e^-\}$$

The stability of such species will be favoured by the defect structure which is so typical for complex solid cyanides. The fact that these species are confined to compounds with a very low content of high-spin iron(III) and a high content of cadmium(II) ions can be explained by the following exchange process:

$$(\alpha)Fe^{II}_{ls} + (\gamma)Fe^{III}_{hs} \quad (\alpha)Fe^{III}_{ls} \cdots e^- \cdots (\gamma)Fe^{III}_{hs}$$
$$(\alpha)Fe^{III}_{ls} \cdots (\gamma)Fe^{II}_{hs}$$

This process, which possibly occurs in all samples, becomes observable in ESR spectroscopy only in those

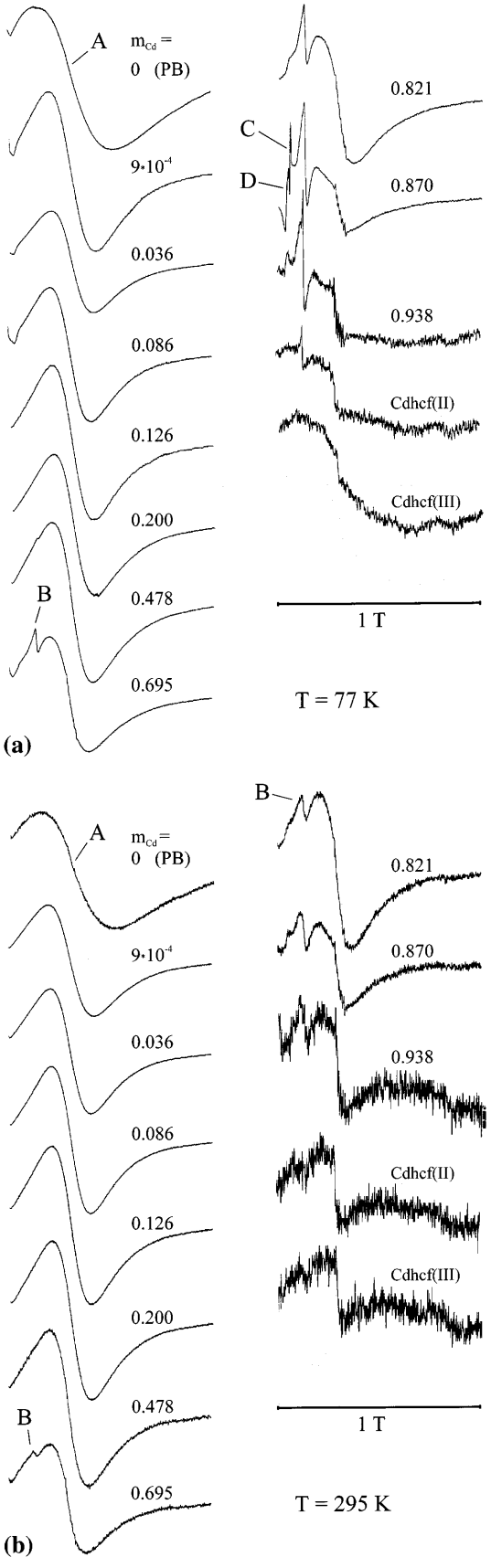

Fig. 11 ESR spectra of $(Fe_{1-x}Cd_x)$ hcf(II) samples for **a** $T = 77$ K and **b** $T = 295$ K

samples which are strongly diamagnetically diluted by cadmium(II). Whether cadmium(II) ions play an active role in this exchange process is still under investigation. In this connection, it is important to remember also that the Mössbauer spectra indicate both Fe^{3+}_{ls} and Fe^{2+}_{hs}. As was deduced already from the magnetic susceptibility, it is also seen here that very small amounts of added cadmium ($m_{Cd} = 9 \times 10^{-4}$) cause a sudden change in the ESR parameters. The width of the resonance line (ΔH) sharply decreases (Fig. 12) after incorporation of the smallest amounts of cadmium ions. As this introduction is accompanied by the fact that almost all interstitial iron(III) is released and substituted by potassium ions, it is possible that the lattice of Prussian blue (PB) assumes a more perfect structure. The initial PB without Cd^{2+} ions may have a much higher concentration of defects as they have been found in PB which was crystallised from hydrochloric acid solution. The decrease of the defect concentration will certainly lead to an increase in the exchange interaction of low-spin Fe^{2+} and high-spin Fe^{3+} sitting at positions α and β in Fig. 2. This assumption is strongly supported by the X-ray diffraction data, which show a remarkable increase in crystallinity when comparing a sample with $m_{Cd} = 0$ to a sample with $m_{Cd} = 9 \times 10^{-4}$. The same has been observed by Reguera et al. [35] in a comparison of insoluble PB and soluble PB. The insoluble PB is practically identical with our sample with $m_{Cd} = 0$, and the soluble PB is practically identical with the sample with $m_{Cd} = 9 \times 10^{-4}$. Usually, it is impossible to achieve a resolution of the resulting overlapping ESR lines [36], but this may be the reason for the broad resonance line in the case of pure PB. Such a situation is easily realised in an "undisturbed" crystal lattice of PB. The distribution of electrons may be disturbed by the introduction of the bigger ions in the unit cell even if their amount is on the level of impurities. Sharper res-

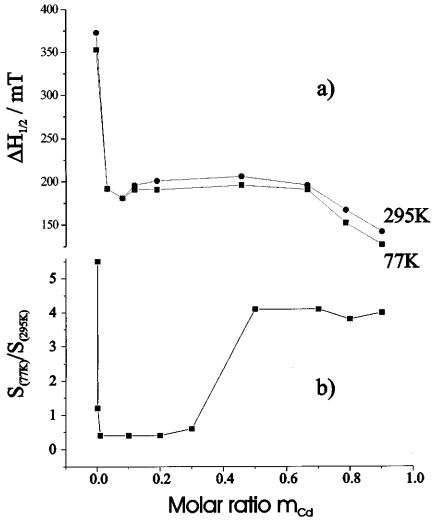

Fig. 12 Plot of **a** the half-width ($\Delta H_{1/2}$) of the resonance line and **b** the ratio of S_{77K}/S_{295K} as a function of the molar ratio m_{Cd} of the $(Fe_{1-x}Cd_x)$ hcf(II) samples

onance lines and more reversible electrochemical reactions are observed in ESR and in electrochemistry, respectively. Plots of $\Delta H_{1/2}$ and $S = (\Delta H_{1/2})^2 I$ (where $\Delta H_{1/2}$ is the half-width, I the intensity of the resonance line, and S the area below the curve of absorption, which is directly connected with the content of paramagnetic centres) versus m_{Cd} (Fig. 12) also exhibit three distinct parts, the borders of which coincide with the introduction of iron or cadmium ions into new positions as implied in the formulas in Table 3 and as is also shown by electrochemical and magnetic measurements.

The simple Curie law according to which the magnetic susceptibility is inversely proportional to temperature is realised only for pure paramagnetic compounds [37]. Figure 12 (curve b) shows the dependence of S_{77K}/S_{295K} on m_{Cd} and indicates that the sample with $m_{Cd} = 0$ has a ratio of $S_{77K}/S_{295K} = 5.5$. This value is above 4, which is the typical value of paramagnetic compounds. Thus, this sample is partially ferromagnetic. It has been shown previously [38] that a sample of the composition $Fe_4^{III}[Fe^{II}(CN)_6]_3 \cdot 15H_2O$ is ferromagnetic at low temperatures with $T_c = 5.5$ K. However, the Fe^{II} ions are low-spin $Fe_{ls}^{II}d^6$ and have $S = 0$. The interaction is weak between the nearest neighbours $Fe_{hs}^{III}d^5$, $S = 5/2$, as the distance is 10 Å. Apparently, the introduction of trace amounts of cadmium perturbs the crystal lattice so much that the orientation of spins which is typical of ferromagnetic materials is lost. It is most likely that the absence of a dependence of $\Delta H_{1/2}$ on temperature and the ratio of $S_{77K}/S_{295K} = 0.4$ for the samples with $0.036 \le m_{Cd} \le 0.200$ and a simultaneous decrease of magnetic susceptibility with m_{Cd} is due to the appearance of antiferromagnetic effects in these phases. The samples with $0.478 \le m_{Cd} \le 0.870$ are paramagnetic because of the ratio of $S_{77K}/S_{295K} = 4.0 \pm 0.2$. Let us remember that the sample with $m_{Cd} = 1.000$ (synthesized with $K_4[Fe(CN)_6]$) is diamagnetic.

Diffuse reflectance spectroscopy

The diffuse reflectance of the MgO diluted samples was measured in the range 400–750 nm and the Kubelka-Munk function K_{KM} was calculated. Figure 13a shows the Kubelka-Munk functions of the samples and Fig. 13b depicts the plot of the K_{KM} maxima versus the composition of the coprecipitates. The diffuse reflectance of the samples decreases by more than 30% when the iron(III) ions at the γ positions are substituted by potassium and cadmium ions. This is another impressive argument for the thesis that the interstitial iron(III) ions are of tremendous importance for the iron(III)-iron(II) interaction in the framework of PB. Although the entire amount of iron at the γ positions is very small compared to the iron(III) content at the β positions, their role in the charge transfer is extraordinary important. One may speculate that the high-spin iron(III) ions at the γ positions are so much more effective for the charge transfer exchange with low-spin iron(II) because they are interacting with four Fe_{ls}^{II} ions, thus making the interaction more effective, and secondly that they are interacting with them more directly and not via cyanide ions.

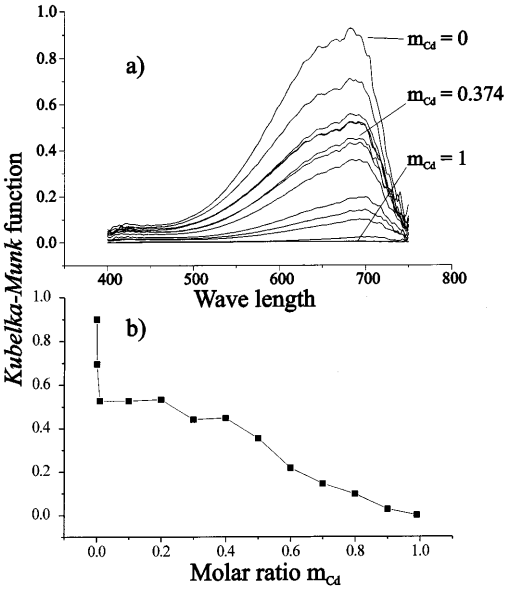

Fig. 13 **a** Kubelka-Munk functions of the cadmium-iron hcf samples (1:50 diluted with MgO); **b** plot of the maximal values of the Kubelka-Munk function versus molar ratio m_{Cd}

Finally, the sample of cadmium hcf(II) with small amounts of iron(III) in the channels exhibits already a spectrum which is very similar to the spectrum of PB. This suggests that iron(III) at the γ positions is able to affect a charge transfer with low-spin iron(II) ions.

Conclusion

The formation of mixed iron-cadmium hcfs can be understood as follows. Small amounts of Cd^{II} ions can be found in the interstitials, i.e. up to 0.15 mol Cd^{II} per mol of hcf. This leads to a distortion of the lattice which makes the "nitrogen holes" (β position in Fig. 2) accessible for Cd^{II} ions. In the undistorted PB lattice, these positions cannot be simultaneously taken by Fe_{hs}^{III} and Cd^{II} because of the different radii of these ions. A further substitution of Fe_{hs}^{III} by Cd^{II} is only possible when the low-spin Fe^{II} is partially oxidised by oxygen and a small fraction of the Fe_{hs}^{III} is even reduced to Fe_{hs}^{II}. In the range $0.478 \le m_{Cd} \le 0.870$ the obtained phase is a very complex mixed crystal. With respect to the interstitial positions, it is a K^I–Cd^{II} mixed crystal. With respect to the hcf sublattice, it is a Fe_{ls}^{II}-Fe_{ls}^{III} mixed crystal [mixed hcf(II)/(III)]. Finally, it is an iron-cadmium mixed crystal with respect to the "nitrogen holes" sublattice, even with an $Fe_{hs}^{II}/Fe_{hs}^{III}$ partition. This study shows the extraordinary important role of interstitial iron(III) ions in PB for the charge transfer between low-spin iron(II) and high-spin iron(III). Finally, and consistent with the latter, the results show that blue colour can be achieved

in cadmium hcf samples when iron(III) ions are only in the channels (at the γ positions).

Acknowledgements N.F.Z. acknowledges support by BMBF which enabled her to undertake this study in Berlin in the framework of a German-Russian collaborative project. F.S. acknowledges support by Deutsche Forschungsgemeinschaft and Fonds der Chemischen Industrie. U.S. was supported by Hans-Böckler-Stiftung.

References

1. Itaya K, Uchida I, Toshima S (1983) J Phys Chem 87: 105
2. Krishnan V, Xidis AL, Neff VD (1990) Anal Chim Acta 239: 7
3. Mortimer RJ, Rosseinsky DR (1983) J Electroanal Chem 151: 133
4. Carpenter MK, Cornell RS (1990) J Electrochem Soc 137: 2463
5. Kobayashi N, Hirohashi R, Ohno H, Tsushida E (1990) Solid State Ionics 40/41: 491
6. Monk PMS, Mortimer RJ, Rosseinsky DR (1995) Electrochromism. Fundamentals and Applications. VCH, Weinheim
7. Kaneko M, Hara S, Yamada A (1985) J Electroanal Chem 194: 45
8. Feldman BJ, Lundgren C, Murray RW (1986) Anal Chem 194: 601
9. Feldman BJ, Melroy OR (1987) J Electroanal Chem 234: 213
10. Kulesza PJ, Chelmecki G, Galadyk B (1993) J Electroanal Chem 347: 417
11. Dostal A, Meyer B, Scholz F, Schröder U, Bond AM, Marken F, Shaw ShJ (1995) J Phys Chem 99: 2096
12. Dostal A, Schröder U, Scholz F (1995) Inorg Chem 34: 1711
13. Siperko LM, Kuwana T (1986) J Electrochem Soc 133: 2439
14. Bharathi S, Joseph J, Jeyakumar D, Prabhakara Rao G (1991) J Electroanal Chem 319: 341
15. Kulesza PJ, Jedral T, Galus Z (1989) Electrochim Acta 34: 851
16. Huheey JE (1988) Anorganische Chemie. Prinzipien von Struktur und Reaktivität. de Gruyter, Berlin
17. Scholz F, Nitschke L, Henrion G (1989) Naturwissenschaften 76: 71
18. Scholz F, Meyer B (1994) Chem Soc Rev 23: 341; Scholz F, Meyer B (1998) Voltammetry of solid microparticles immobilized on electrode surfaces. In: Bard AJ, Rubinstein I (ed) Electroanalytical chemistry, a series of advances, vol 20. Dekker, New York p 1
19. Zakharchuk NF, Meyer B, Hennig H, Scholz F, Jaworski A, Stojek A (1995) J Electroanal Chem 398: 23
20. Scholz F, Dostal A (1995) Angew Chem 107: 2876; (1995) Angew Chem Int Ed Engl 34: 2685
21. Reddy SJ, Dostal A, Scholz F (1996) J Electroanal Chem 403: 209
22. Dostal A, Hermes M, Scholz F (1996) J Electroanal Chem 415: 133
23. Dostal A, Kauschka G, Reddy SJ, Scholz F (1996) J Electroanal Chem 406: 155
24. Gmelin Handbuch der Anorganischen Chemie (1932) 8th edn, vol 58B (Fe). Verlag Chemie, Berlin, p 1108
25. Selvud P (1962) Adsorption and collective paramagnetism. Academic Press, New York
26. Schröder U, Scholz F (1997) J Solid State Electrochem 1: 62
27. Tananaev IV, Seifert GB, Kharitinov YuYa, Kuznetsov VG, Korolkov AP (1971) Khimiya ferrocyanidov (in Russian). Nauka, Moscow
28. Ludi A, Güdel H-U (1973) Structure Bonding 14: 1
29. Seifer GB (1962) Zh Neorg Khim 7: 621
30. Volkhin VV, Schulgar MB, Silberman MV (1971) Izv Akad Nauk Neorg Mater 7: 77
31. Luangdilok CH, Arent DJ, Bocarsly AB, Wood R (1992) Langmuir 8: 650
32. Williams HE (1948) Cyanogen compounds, 2nd edn. Arnolds, London
33. Davidson D, Welo D (1928) J Phys Chem 32: 1192
34. Brückner A, Wolf G-U, Meisel M, Stösser R, Mehner H, Majunke F, Baerns M (1995) J Catal 154: 11
35. Reguera E, Bertràn JF, Nunez L (1994) Polyhedron 13: 1619
36. Atkins PW, Symons MCR (1967) The structure of inorganic radicals. Elsevier, Amsterdam
37. West AR (1992) Grundlagen der Festkörperchemie. VCH, Weinheim
38. Mallah T, Thiebault S, Verdaguer M, Veillet P (1993) Science 262: 1554